International Journal of Environmental Science and Technology (2024) 21:3789–3802
https://doi.org/10.1007/s13762-023-05245-5

ORIGINAL PAPER

Adsorption of methylene blue by composite foams containing alkali-activated blast furnace slag and lignin

M. A. H. Bhuyan[1] · **T. Luukkonen**[1]

Received: 28 March 2023 / Revised: 23 August 2023 / Accepted: 21 September 2023 / Published online: 16 October 2023

Abstract

Adsorption is a promising method to remove dyes, such as methylene blue, from wastewater. In this study, a dynamic adsorption set-up was used to treat synthetic wastewater containing methylene blue by using alkali-activated blast furnace slag and lignin composite foam. The structure of the foam without lignin was first optimized by comparing cationic and non-ionic surfactants in the preparation of the foam via the direct foaming method. The selection of the surfactant affects the porosity and pore structure of the foam through different abilities to stabilize the gas–liquid interface and changes in the viscosity of the fresh-state paste. The foam prepared with non-ionic Triton X-114 surfactant had the highest adsorption performance and was selected for the optimization of adsorption conditions. The optimized conditions were 5 mg/L influent concentration of methylene blue, pH of 7, and flow rate of 1.0 L/h (corresponding to ~ 9 min empty bed contact time). To further enhance the methylene blue adsorption performance, a composite containing lignin was prepared. The optimum lignin amount in the foam was 0.8 wt% and it resulted a ~93% higher adsorption amount compared to the foam without lignin. The highest cumulative adsorption capacity in this dynamic adsorption setup was 39.5 mg/g, which is among the highest reported values for methylene blue removal by monolithic adsorbents. The present study provides a proof of concept for the enhancement of adsorption performance of alkali-activated materials by introduction of lignin into the structure.

Keywords Alkali-activated materials · Direct foaming · Dye · Geopolymers · Wastewater treatment

Introduction

Water is a prerequisite for all forms of life and most industrial activities. Thus, the need for clean water is increasing due to the increase of world population, changes in the global water cycle caused by the climate change, and the deterioration of water quality in several areas. One source contamination for water resources are heavy metals and persistent organic pollutants such as dyes, detergents, or petroleum products, to name just a few examples (Gautam et al. 2014; Raza et al. 2019; Quesada et al. 2019; Zamora-Ledezma et al. 2021; Ortúzar et al. 2022; Luukkonen et al. 2022).

Synthetic dyes are utilized extensively in different sectors such as the paint, printing, textiles, leather, plastics, cosmetics, food colouring, and pharmaceutical industries (Rezaei and Salem 2016; Pang et al. 2017). Currently, over one hundred thousand commercial dyes are available with a combined production of approximately 700,000 tonnes in each year (Kaya-Özkiper et al. 2022a). Dyes can include acidic, basic, azo, and diazo moieties or can be based on metal complexes (Hunger 2007; Chavan 2011). Approximately 10–15% of the dyes are discharged into water without any treatment, which has adverse impacts on the aquatic environments and, subsequently, on the health of human populations (Chan et al. 2015; Hussain et al. 2020). Dye concentrations even lower than 1 mg/L can be visually observable and unhealthy for human consumption (Moradihamedani 2022). Many of the commercial dyes are not biodegradable, and thus remain highly stable in the environment (Joseph et al. 2019). Moreover, some dyes (e.g., Disperse Blue 373, Disperse Orange 37, and Disperse Violet 93) can be carcinogenic or mutagenic (Alves de Lima et al. 2007; Subramanian et al. 2022). The presence of dyes in

Editorial responsibility: Agnieszka Galuszka.

✉ M. A. H. Bhuyan
mohammad.bhuyan@oulu.fi

[1] Fibre and Particle Engineering Research Unit, University of Oulu, Erkki Koiso-Kanttilan Katu, 90014 Oulu, Finland

water interrupts the penetration of light (Pandey et al. 2007) and also causes increased biochemical and chemical oxygen demand (Yao et al. 2009).

Methylene blue (MB), a basic cationic dye, is one of the most widely consumed dyes in several industries (Parakala et al. 2019; Koyuncu and Kul 2020; Khan et al. 2022). MB is also used in microbiological staining and as pharmaceutical compound where the safe dose is less than 2 mg/kg of body weight (Ginimuge and Jyothi 2010; Wainwright et al. 1997). Chronic exposures to high MB concentrations (> 2 mg/kg) can cause low blood pressure, gas exchange deterioration in the lungs, abnormal heartbeat, coronary vasoconstriction, increased pulmonary vascular pressure, or pulmonary vascular resistance (Ginimuge and Jyothi 2010). The concentration of MB found in typical wastewaters generated by the textile industry is between 10 and 200 mg/L (Kadam et al. 2011). Water contamination by MB has been recognized as one reason for the shortage of clean water in the affected areas (Walker et al. 2019; Oladoye et al. 2022). MB produces a highly coloured solution even at a very low concentration in an aquatic environment (Khan et al. 2022). Because of the high molar absorption coefficient value of MB [$\sim 8.4 \times 10^4$ L/(mol × cm)], it can decrease the transmittance of sunlight through the water and, consequently, disturb the photosynthesis of aquatic organisms (Kosswattaarachchi and Cook 2018; Khan et al. 2022). MB-contaminated water, depending on the concentration and exposure duration, can have acute effects on human health, for example causing vomiting, diarrhoea, nausea, or difficulties in breathing (Gupta and Suhas 2009; Banerjee et al. 2015).

Various techniques including membrane separation, chemical or electrochemical oxidation, (electro-)coagulation and flocculation, adsorption, photodegradation, biological treatment, or combinations of these have been investigated to remove MB from aquatic environment (Hou et al. 2018; Cheng et al. 2020; Ahmed et al. 2022). Adsorption technology is considered a promising method to remove MB because of its simplicity in use, low operational costs, and potential high efficiency (Kuang et al. 2020; Eldeeb et al. 2022; Ye et al. 2023). However, further research is required to find more environmentally friendly, low cost, and efficient adsorbents.

Alkali-activated materials (AAMs), and geopolymers (a subclass of AAMs), are mainly utilized and studied for the construction material applications at the moment, but they have also several high-value uses such as materials for water treatment (Luukkonen et al. 2022). Alkali activation is a process in which aluminosilicate precursors (e.g., calcined clays, metallurgical slags, or fly ashes) and an alkali activator solution (e.g., alkali metal hydroxide, silicate, or carbonate) react at low temperature (< 100 °C) to form aluminosilicate products. Blast furnace slag (BFS), a by-product from iron manufacturing, is one of the typical precursors used for the preparation of high-calcium-content AAMs (Aziz et al. 2020). The availability of BFS is expected to decrease in the near future as the steel industry transitions into the reduction of iron ore by H_2 instead of coke and using electric arc furnaces to further process the formed sponge iron (Patisson and Mirgaux 2020). Nevertheless, BFS can be replaced by other high-Ca content aluminosilicate precursors in the future. Therefore, BFS-based AAMs can be considered as useful model systems of those containing calcium/sodium–aluminium–silicate–hydrate gels (or C/N–A–S–H in the cement chemist notation). BFS-based alkali-activated materials have drawn attention for their environmental applications, for example as adsorbents in wastewater treatment (Luukkonen et al. 2016; Runtti et al. 2016; Medina et al. 2020; Sundhararasu et al. 2021; Humberto Tommasini Vieira Ramos et al. 2022; Abdelbasir and Khalek 2022). Gheibi et al. (2022) and Eftekhari et al. (2021) have earlier reported excellent adsorption performance of aerated autoclaved concrete (where the predominant phase is calcium–silicate–hydrate, C–S–H) and its composite with chitosan for cationic dyes malachite green, methyl violet, and MB (maximum adsorption capacities between 256–833 mg/g for powders). Their works are highly encouraging related to the present study since the BFS-based AAM consists essentially aluminum-substituted C–S–H (i.e., C–A–S–H).

Alkali-activated highly porous materials are a new emerging topic related to the use of AAMs as adsorbents since they can be regenerated more readily and require no separation steps unlike powder-form adsorbents. The direct foaming method is commonly used to prepare alkali-activated porous materials (Bai and Colombo 2018): there, a blowing agent, such as hydrogen peroxide (H_2O_2), peracetic acid (CH_3COOOH), or metallic aluminium (Al^0), is used to introduce pores to the AAMs, and a surfactant is used to prevent the coalescence of bubbles (Bai and Colombo 2018; Bhuyan et al. 2023).

Alkali-activated BFS (AABFS) has already been proven as a promising adsorbent for water and wastewater treatment (Luukkonen et al. 2016; Runtti et al. 2016; Latorrata et al. 2021; El Alouani et al. 2021). The development of solid foam by alkali-activation of BFS with the direct-foaming method and its use as an adsorptive filter in wastewater treatment was reported earlier (Bhuyan et al. 2022). From this work, it was observed that surfactants greatly influence the properties of AABFS foam, for example, porosity, but the effect of different types of surfactants used in the AABFS foam preparation on the adsorption performance is not studied in detail. The use of different surfactants is expected to impact the porosity and pore structure of the foams through the change of viscosity of the fresh-state paste resulting from the reaction of the surfactants with soluble compounds, which can cause differences in the adsorption performance.

Lignin is a component of wood that is obtained as a by-product from pulp production and is mainly used as a fuel for power and heat generation (Sharma et al. 2021). The amount of lignin generated from the pulp industry is more than 70 million tonnes annually (Saad and Hawari 2013). It is, after cellulose, the second most abundant natural biopolymer, comprising 18–35 wt% of wood (Shorey et al. 2021). Globally, the availability of lignin in the biosphere is approximately 300 billion tonnes (Bajwa et al. 2019; Shorey et al. 2021). Because of the presence of numerous functional groups, for example, ether, carbonyl, aliphatic, and aromatic hydroxyl groups, lignin can have various chemical interactions with different pollutants (such as MB) via electrostatic interaction, H-bonding, and π–π interactions (Suteu et al. 2010). The application of lignin as an adsorbent in removing different pollutants, for example, dyes, potentially toxic elements, or pesticides from water has been reported (Mariana et al. 2021; Wang et al. 2022). The addition of lignin to AAMs to form a composite has been also reported (Ye et al. 2018), but the application of such biomass-AAM composites for wastewater treatment has been investigated only to a very limited extent, and thus represents a research gap. It is hypothesized that the introduction of additional functional groups to the surface via the development of composite materials would increase the adsorption performance of AAMs via enhanced and more diverse molecular interactions between the AAM composite surface and adsorbates (Açışlı et al. 2022).

The main target of the present study is to introduce lignin to the AABFS structure to enhance the adsorption capacity of MB in a dynamic adsorption set-up. The first part of the study addresses the AABFS foam without lignin by (a) selecting the optimum surfactant type (cationic or non-ionic) based on the adsorption performance of MB in a dynamic adsorption set-up; (b) optimizing the factors affecting adsorption: pH, flow rate, and initial concentration of MB; and (c) characterization (by infrared spectroscopy and zeta potential measurements) of the AABFS foams before and after MB adsorption and after thermal regeneration. In the second part of the study, the optimum lignin amount in AABFS foam is selected based on compressive strength, porosity, and specific surface area characterization. The optimized lignin-containing AABFS is used in dynamic adsorption experiments to observe breakthrough curves in comparison to AABFS foam without lignin. The breakthrough curves were fitted to kinetic models, namely, Adams–Bohart, Thomas, and Yoon–Nelson models. This is the first study in which a lignin-AAM composite material is applied for an adsorption application providing insights about the significant improved adsorption performance. This study was carried in Oulu, Finland from October 2021 to November 2022.

Materials and methods

This section is divided into sub-sections describing the used raw materials and chemicals, preparation of alkali-activated foams and introduction of lignin, material characterization methods, and adsorption experiments conducted with MB.

Materials and chemicals

The BFS used in this study (tradename KJ400) was obtained from Finnsementti (Finland), and its composition (in wt%) is 38.5% CaO, 32.3% SiO_2, 9.5% Al_2O_3, 10.2% MgO, 4.0% SO_3, and 1.2% Fe_2O_3. The alkali activator was prepared by stirring a Na_2SiO_3 solution (Merck, extra pure, molar $SiO_2/Na_2O \approx 3.5$, 65 wt% water) and NaOH pellets (98.7%, VWR) to obtain a SiO_2/Na_2O molar ratio of approximately 1.2 and the amount of water approximately 56 wt%. H_2O_2 (30%, VWR, w/v) was used as a blowing agent, and four different surfactants—Triton X-405 (70% solution, Sigma-Aldrich), Triton X-114 (100% solution, VWR Acros), Triton X-100 (100% solution, VWR), and cetyltrimethylammonium bromide (CTAB; ≥ 99 wt% solid, VWR)—were employed in the preparation of foams. Among these surfactants, Triton surfactants are non-ionic and CTAB is a cationic surfactant. The non-ionic surfactants have a difference in their ethylene oxide chain length and cloud point; the chain length of Triton X-114 is the shortest while Triton X-100 is the longest, and Triton X-405 has the highest cloud point among all three. Methylene blue (MB, TCI, ˃ 70%) was used to prepare synthetic wastewater, and lignin (alkaline, VWR TCI) was used to functionalize the AABFS. MB solutions of three different pH were prepared by using a buffer solution of pH 4 (0.1 M acetic acid buffer), 7 (0.05 M phosphate buffer), and 9 (0.05 M bicarbonate buffer).

Preparation of AABFS with different surfactants

The preparation of AABFS foams were conducted by the direct foaming method (Bhuyan et al. 2022). BFS, alkali activator solution and water were mixed for 4 min with a high-shear mixer (IKA EUROSTAR 20) using a speed of 3000 rpm. H_2O_2 (0.06 wt% of paste) and four distinct surfactants—CTAB, Triton X-100, Triton X-405, and Triton X-114 (0.001 mmol/g paste)—were added, and mixing (speed 3000 rpm) was continued for additional 2 min. Then, the paste was cast in column moulds of diameter 4.3 cm and length 10.2 cm and curing was done at 60 °C inside the oven for 4 h by keeping it in an airtight bag. In the next step of curing, the airtight bag containing the samples was stored at room temperature. Before their use in the adsorption experiments, the neutralization of the pore solution of the foams was done by using 0.1 M acetic acid.

Preparation of AABFS-lignin (AABFS-Lig) composite foams

To prepare the AABFS-Lig composite foam, different percentages (0–1 wt% of the precursor) of alkaline lignin (VWR TCI) were mixed with BFS for 1 min, then the alkali activator solution and water were added in, and mixing was continued for 4 min to get a homogeneous paste. Next, H_2O_2 and Triton X-114 were poured in the paste and mixed (speed 3000 rpm) for additional 2 min. Triton X-114 was used with composite foams based on the comparative adsorption experiments between the foams prepared with different surfactants. The paste containing lignin was cast, cured, stored, and pre-treated similarly as described above.

Characterization of the AABFS and AABFS-Lig foams

Mechanical strength

Foam samples (50 mm × 50 mm × 40 mm) were characterized for compressive strength by employing a universal testing machine, ZwickRoell Z10 (10 kN), with 1 mm/min loading rate. The measurement was carried out for 3 replicates at 7 d sample age. Equation (1) was employed to determine the compressive strength (σ, [MPa]) of the foam samples:

$$\sigma = \frac{F}{A} \tag{1}$$

here A indicates the surface area (mm^2) under compression, and F is the force (N).

Fourier transform infrared spectroscopy (FTIR)

The alteration in the chemical environment of the AABFS after neutralization with acetic acid, and MB adsorption were studied by FTIR (Bruker VERTEX 80v). Powdered samples (particle size < 500 µm) were used for the analysis, and the wavenumber range during the collection of spectra was 500–4500 cm^{-1} and resolution was 2 cm^{-1}. In the similar way, the change in the chemical environment of AABFS-Lig before and after adsorption of MB was studied.

BJH and BET

Nanometer-scale pore volume and the surface area of the foams were studied by applying the Barrett–Joyner–Halenda (BJH) method and the Brunauer–Emmet–Teller (BET) isotherm for the adsorption and desorption of liquid N_2 at − 196 °C. A Micromeritics ASAP 2020 instrument was employed for this analysis. Before measurement, the foam samples were crushed into 4–8 mm pieces, freeze-dried for 72 h, then degassing of the samples was conducted at 70 °C for 24 h.

He-gas pycnometry

A helium gas pycnometer of model AccuPyc II 1340 (Micromeritics) was used to investigate the open and total porosity of the prepared foam samples. Dried foam samples (at 60 °C) were used to calculate the geometric density (ρ_g [g/cm^3]) by determining sample dimensions and their mass by using a calliper and analytical balance, respectively. The helium gas pycnometer was used to determine the apparent density (ρ_a [g/cm^3]) and true density (ρ_t [g/cm^3]) from crushed foam particle sizes of < 1 cm and < 500 µm, respectively. Equations (2, 3) were employed to calculate the open and total porosities, respectively.

$$\text{Open porosity } [\%] = \frac{\rho_a - \rho_g}{\rho_a} \times 100 \tag{2}$$

$$\text{Total porosity } [\%] = \frac{\rho_t - \rho_g}{\rho_t} \times 100 \tag{3}$$

Zeta potential analysis

A Zetasizer pro (Malvern) was employed to determine the zeta potentials of the AABFS foams at pH of 4–9. The powders (0.1 wt%, particle size ≤ 100 µm) were dispersed in 0.1 M HCl, and the dispersion was used for the zeta potential measurements. NaOH and HCl were used to adjust pH.

Adsorption experiments

MB adsorption by AABFS foams using different surfactants

To compare the MB adsorption performance by AABFS foams prepared with different surfactants, the foams were cast in column moulds of diameter 4.3 cm and length 10.2 cm. The geometric density of the foams was 0.85–1.13 g/cm^3 depending on the selection of the surfactant (see Table S1, Supporting information, SI). It should be noted that the weights of the foams were detected after curing without drying, and thus they also contain some contribution from water (~ 2 wt%) (Bhuyan et al. 2022). These values were used to calculate the adsorbed amount of MB per mass of the adsorbent (referred from this on as an adsorption amount). The foams were neutralized by using 4 L of 0.1 M acetic acid and 4 L of deionized water by pumping them through the foam with a 1.0 L/h flow rate. A

5 mg/L MB solution was prepared in a 0.05 M phosphate buffer. A peristaltic pump (MINIPLUS 3) was used to distribute 6 L of MB solution through the foam with a flow rate of 1.0 L/h (i.e., empty bed contact time ≈ 9 min). Using 15 min intervals, the filtrate was collected and analysed immediately by using a Shimadzu UV-1800 ultraviolet–visible light (UV–Vis) spectrophotometer at a wavelength of 664 nm. Calibration was conducted for the MB solutions in a concentration range of 1 to 5 mg/L, as shown in Fig. S1 (SI). Based on these experiments, an AABFS prepared with Triton X-114 surfactant was chosen for the optimization of flow rate (0.5 or 1.0 L/h), pH (4, 7, or 9) and influent concentration of MB (5, 10, 15, or 20 mg/L). The cumulative adsorption amount per mass of the foam, q_t (mg/g) was determined by employing Eq. 4. However, it should be noted that the cumulative adsorption amount does not reflect the maximum adsorption capacity of the foam as complete saturation was not reached.

$$q_t = \frac{Q \int_0^t (C_0 - C_t) dt}{m} \quad (4)$$

In Eq.(4), C_0 (mg/L) indicates the concentration of the influent, C_t (mg/L) indicates the concentration of the effluent at time t (min), and m (g) indicates the mass of the foam after curing including the contribution of water (~2 wt%).

MB adsorption by AABFS-Lig

AABFS-Lig composite foams with different percentages of lignin (0.0–0.8 wt%) were prepared and tested similarly as described above. The geometric densities of these foams were 1.05–0.63 g/cm^3 (i.e., higher lignin content decreased the density), as shown in Table S2 (SI). Based on the highest cumulative adsorption amount, the optimum AABFS-Lig composite foam (i.e., with 0.8 wt% of lignin) was chosen to investigate the effect of different initial concentrations of MB. Throughout all experiments, the flow rate of 1.0 L/h, and a pH of 7 were maintained.

Kinetic models

For scaling-up the column adsorption process, the prediction of the breakthrough curve is significant. To study the kinetics of a continuous fixed adsorption column, Adams–Bohart, Thomas, and Yoon–Nelson models (Eqs. 5–7 respectively) were employed in the prediction of breakthrough curve behaviour (Bohart and Adams 1920; Thomas 1944; Yoon and Nelson 1984):

$$\ln\frac{C_t}{C_0} = k_{AB}C_0 t - k_{AB}N_0\frac{Z}{F} \quad (5)$$

In Eq. (5) (i.e., the Adams–Bohart model), k_{AB} [L/(mg × min)] indicates the rate constant, F (cm/min) indicates the linear-flow velocity, N_0(mg/L) indicates the adsorption capacity of the adsorbent per unit volume of the bed, Z (cm) indicates the bed height, and C_0 and C_t indicate concentrations of inlet MB and effluent MB, respectively (mg/L).

$$\ln\left(\frac{C_0}{C_t} - 1\right) = \frac{k_{Th}q_0 w}{Q} - k_{Th}C_0 t \quad (6)$$

In Eq. (6) (i.e., the Thomas model), k_{Th} [L/(mg × min)] indicates the rate constant, q_0 (mg/g) indicates the adsorption capacity of the bed at the breakthrough point, and w indicates the mass of the bed (g).

$$\ln\frac{C_t}{C_0 - C_t} = k_{YN}t - \tau k_{YN} \quad (7)$$

In Eq. (7) (i.e., Yoon–Nelson model), k_{YN} (1/min) indicates the rate constant, τ (min) indicates the time required for the breakthrough of 50% adsorbate, and t (min) indicates the breakthrough time.

To determine the Adams–Bohart, Thomas, and Yoon–Nelson models parameters, a nonlinear regression was performed by employing the Microsoft Excel Solver function (GRG nonlinear).

Results and discussion

This section is divided into two sub-sections describing the AABFS foam optimization, characterization, and application for MB adsorption without lignin and introduction of lignin to the foam and comparing the properties to the foam without lignin.

Optimization and characterization of AABFS foam without lignin

Selection of the optimal surfactant when preparing AABFS foams

Three non-ionic surfactants (Triton X-100, X-114, and X-405) and one cationic surfactant (CTAB) were used to prepare AABFS foams. The presence of different functional groups in non-ionic and cationic surfactants can modify the surface charge and bubble stability in the fresh-state geopolymer paste and, consequently, could have an effect on viscosity (Perumal et al. 2021). From earlier studies, it is known that CTAB produces higher porosity and specific surface area in comparison to non-ionic surfactants (Bhuyan et al. 2022). Due to this higher specific surface area and porosity, it is expected that AABFS foam with CTAB would show better performance in MB adsorption compared to other

non-ionic surfactants. However, MB is positively charged at neutral or basic pH, similarly as CTAB, and, thus, there would be a repulsion between them that could have a negative influence on MB removal (Kuang et al. 2020).

The results obtained for MB removal by using AABFS foam prepared with different surfactants are presented in Fig. 1. The duration of the experiment for MB was 6 h with a flow rate of 1.0 L/h, initial MB concentration of 5 mg/L, and pH of 7. The foam prepared with Triton X-114 had the highest MB adsorption amount, possibly due to its highest specific area. MB removal (as %) by AABFS foam prepared with different surfactants are presented in Fig. S2 (SI), where AABFS foam prepared with Triton X-114 still had ~ 84% removal efficiency after 6 h. Thus, the cumulative adsorption amount reported in Fig. 1 does not represent the maximum adsorption capacity.

Optimizing the adsorption conditions: initial MB concentration, flow rate, and pH

The effect of changing the influent concentration of MB from 5 to 20 mg/L when using the Triton X-114-based AABFS foam is presented in Fig. 2. A representative concentration of MB in textile industry wastewater is typically between 10 and 200 mg/L (Kadam et al. 2011). With the increase of the initial concentration of MB, the cumulative adsorption amount of AABFS (again, the cumulative adsorption amount was calculated after 6 h of continuous adsorption experiment) increased. The likely reason for the increased adsorption when increasing the influent concentration of MB is that the mass transfer driving force (concentration gradient) is enhanced (Nasuha et al. 2010). After a 6 h experiment, the MB removal (as %) in the influent concentration range of 5–15 mg/L dropped by approximately 14–15%, whereas for the influent concentration of 20 mg/L, it dropped by approximately 20% from the initial value of 100% (Fig. S3, SI). This decrease is likely due to coverage of adsorbent active sites with MB molecules (Ebadollahzadeh and Zabihi 2020).

The effect of flow rates (i.e., 0.5 and 1.0 L/h corresponding to ~ 18 and ~ 9 min empty bed contact times, respectively) of MB solution (5 mg/L) on the adsorption efficiency and cumulative adsorption amount of AABFS over 6 h at pH 7 are shown in Fig. S4 (SI). Enhanced MB adsorption was observed with a lower flowrate or longer empty bed contact time, which is a typical behaviour for dynamic adsorption systems (Sittipol et al. 2021). Longer contact time allows more mass transfer of MB to occur into the pores of the foam materials (Cruz-Olivares et al. 2013).

MB adsorption on AABFS prepared with Triton X-114 at pH 4, 7, or 9 was investigated by distributing 6 L of MB solution of 5 mg/L through the foam with a flow rate of 1.0 L/h, as shown in Fig. 3. The duration of the experiment was 6 h. At pH 9, a slightly higher extent of MB adsorption was observed compared to pH 7, which could be because of a more negative surface charge at pH 9 (as shown in Fig. S5, SI). The electrostatic attractions or repulsions between the surface of the foam and MB species in the solution are dependent on pH. At pH 7 and 9, methylene blue exists 100% in a cationic form, but at pH 4 it is approximately 50% in non-ionic undissociated form (Salazar-Rabago et al. 2017). At pH 7 and 9, the cationic MB species are adsorbed by the negatively charged surface of the foam. Surprisingly, however, the highest MB adsorption amount by the foam was found at pH 4, although the surface of the foam is positively charged. This indicates that the foam can possibly adsorb undissociated MB molecules at pH 4, which could be because of another mechanism (e.g. hydrogen bonding) rather than electrostatic interaction (Eldeeb et al. 2022). A similar finding, that is, the highest MB adsorption at pH 3 compared to pH of 4–8, was reported for MB adsorption by the geopolymer prepared from rice husk ash, metakaolin,

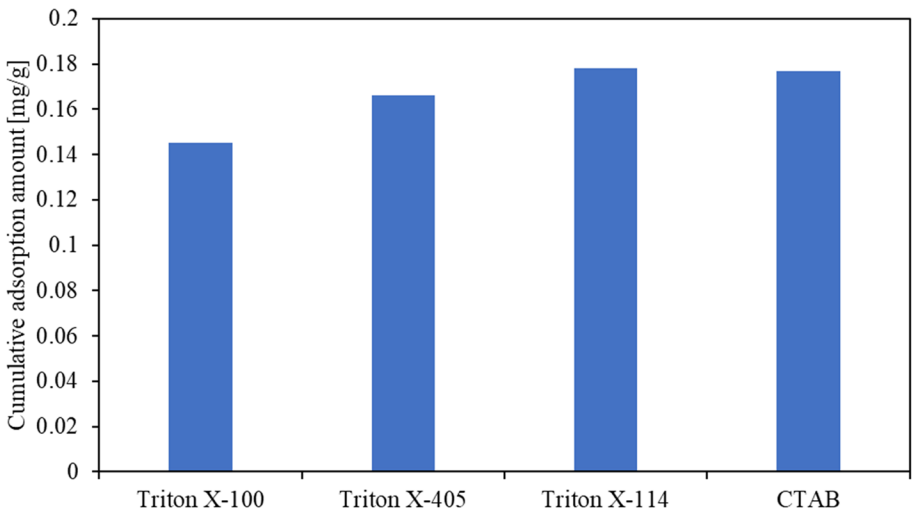

Fig. 1 Comparison of the cumulative adsorption amount of MB after 6 h adsorption experiment by AABFS foams prepared with different surfactants. The other parameters of the experiment were: flow rate of 1.0 L/h, initial MB concentration of 5 mg/L, and pH of 7

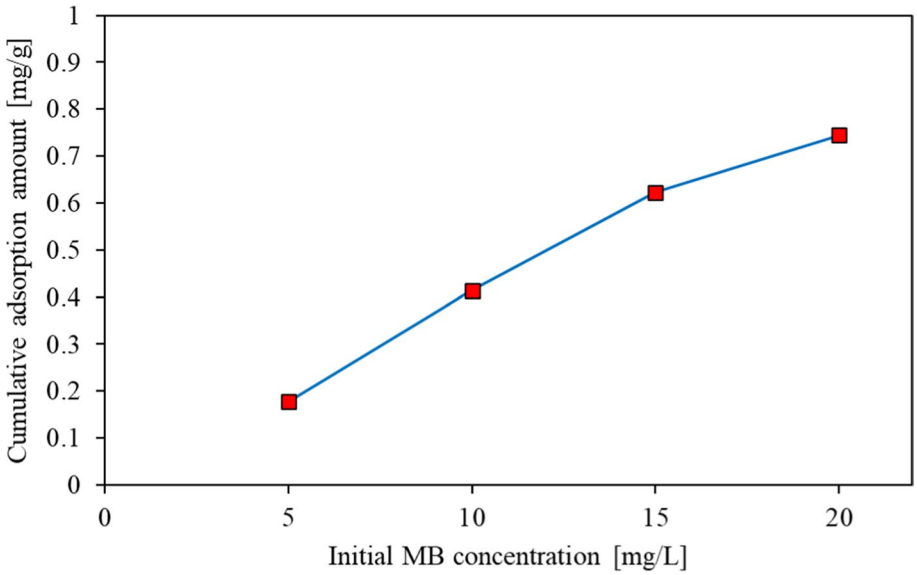

Fig. 2 The effect of initial MB concentration on cumulative adsorption amount (calculated after 6 h of experiment) of AABFS foam prepared with Triton X-114 surfactant. The other parameters of the experiment were: flow rate of 1.0 L/h and pH of 7

palm oil fuel ash, and ground granulated blast furnace slag (Maleki et al. 2020). The MB removal by AABFS for pH 4, 7, and 9 were approximately 84–100%, as shown in Fig. S6 (SI).

Characterization of the AABFS foams before and after MB adsorption

The FTIR spectra of AABFS foam (prepared with the Triton X-114) before and after neutralization with acetic acid, and after MB adsorption are shown in Fig. 4. In every case, the bands at ~ 3475 cm^{-1}, ~ 2350 cm^{-1}, and ~ 1650 cm^{-1} are the stretching and bending vibration of hydroxyl groups on the foam surface caused by adsorbed water molecules (Puertas et al. 2011; Razeghi et al. 2022). The band at ~ 1425 cm^{-1} is from the carbonation of the AABFS foam surface (Cao et al. 2020). The band at ~ 1125 cm^{-1} (i.e. Si–O–Si/Al stretching (Bernal et al. 2015)) shifted towards a higher wavenumber after acetic acid-washing, or adsorption of MB, which indicates changes in the chemical structure. After MB adsorption, two weak bands at ~ 2500 cm^{-1} and ~ 1750 cm^{-1} appear, which are from the MB structures, namely C_{het}–$N(CH_3)_2$ vibrations and $C_{het}=N^+(CH_3)_2$ stretching vibrations (where C_{het} is a carbon atom in the heterocycle of MB) (Ovchinnikov et al. 2016).

The zeta potential of the AABFS foam prepared with a Triton X-114 surfactant was measured at pH of 4, 7, and 9, and the results are presented in Fig. S5 (SI). The point of zero charge for the foam was observed at pH 4.8 (i.e., the overall surface charge is zero), and thus the surface has

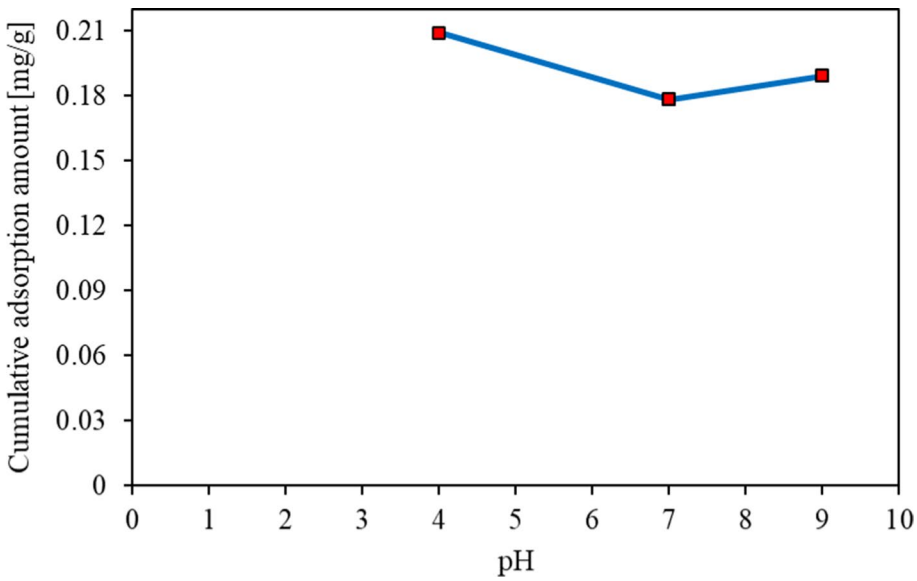

Fig. 3 The effect of solution pH on the MB adsorption capacity (cumulative adsorption amount was calculated at 6 h) by the AABFS foam prepared with Triton X-114 surfactant. The other parameters of the experiment were: initial concentration of 5.0 mg/L and flow rate of 1 L/h

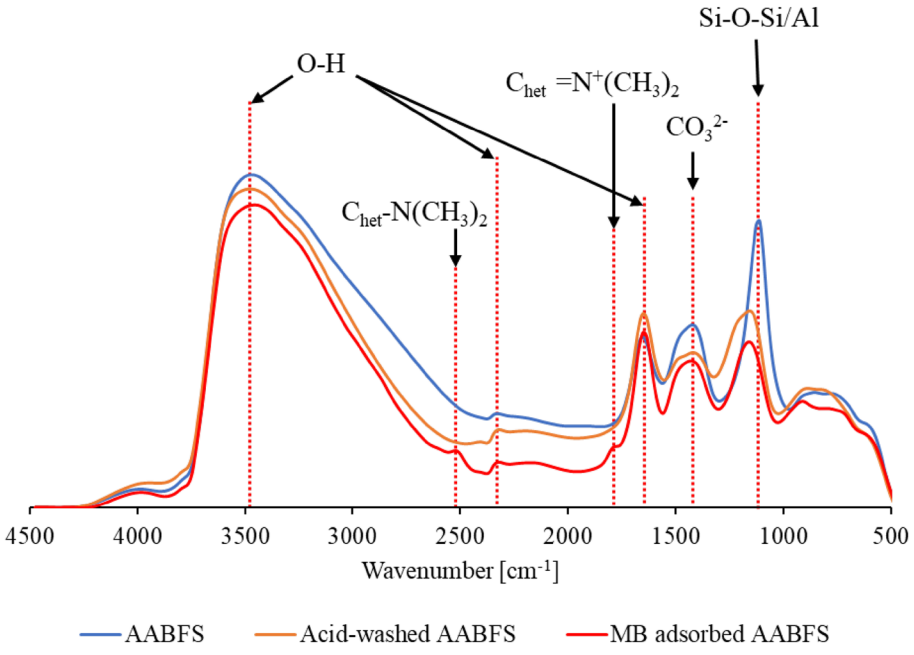

Fig. 4 FTIR spectra of the AABFS foam prepared with Triton X-114 surfactant before and after 0.1 M acetic acid washing and after MB adsorption (conducted with acid-washed AABFS). C_{het} = carbon atom in the heterocycle structure of MB

a positive charge when pH is < 4.8 and a negative charge when pH is > 4.8. The negative surface charge of AABFS at pH > 4.8 is approximately similar to the other alkali-activated materials (Gunasekara et al. 2015; Hertel et al. 2019). Thus, it is expected that at pH greater than 4.8, the foam can adsorb cationic MB dye via electrostatic interaction. As the pH increases from 7 to 9, the surface is yet more negatively charged, resulting in improved adsorption as reflected in the results of the pH optimization experiments (Fig. 3). The zeta potential of AABFS with the other three surfactants (Triton X-100, Triton X-405, and CTAB) was − 16.3 mV, − 17.5 mV, and − 17.5 mV, respectively, at pH 7.

Introduction of lignin into the AABFS foams

Compressive strength of AABFS-Lig composites

The first selection criteria for the addition amount of lignin (0−1 wt% of the precursor) was the compressive strength of the foam (from this on, Triton X-114 was used to prepare all foam samples) as shown in Fig. 5. Compressive strength was used as a rough indication of the mechanical durability of the foams, that is, to remain intact in flowing water. There were no clear changes in compressive strength up to the addition of 0.8 wt% of lignin compared to AABFS without lignin; however, a reduction in compressive strength for the addition of 1.0 wt% of lignin was clear. The compressive strength of the foam samples depends on their porosity and the shape and size of pores (Ye et al. 2018). The reduction in compressive strength for the addition of lignin higher than 0.8 wt% could be because of a poor integration of lignin into the AABFS structure at high addition amounts.

Porosity and specific surface area of AABFS-Lig composites

The apparent densities and porosities of AABFS foams with different addition amounts of lignin are shown in Table S3 (SI). The apparent density of AABFS foam without lignin was 2.33 g/cm^3, and after the addition of lignin up to 1 wt%, no clear changes were observed. However, the addition of lignin decreased the specific surface area of foams from 86.48 m^2/g to 72.13 m^2/g when the lignin amount was increased from 0 to 0.8 wt%, respectively. The cumulative nano-scale pore volume (Fig. S7, SI) was, in all cases, mainly within 2–30 nm-sized pores (i.e., mesopores). On the other hand, a slight increase in total porosity (as measured with the helium gas pycnometer) was observed after the incorporation of different amount of lignin into the foams. The AABFS foam with 0.8 wt% lignin showed ~ 74% total porosity whereas without lignin it was ~ 69%. In all cases, the open porosity and the total porosity were almost equal, which indicated that the pores in the foams were connected (Bhuyan et al. 2022).

MB adsorption with AABFS-Lig composites

AABFS-Lig composites with different amounts of lignin (0–0.8 wt%) were employed for MB removal from MB solution with a concentration of 5 mg/L and pH of 7 (Fig. 6). The composite with 1.0 wt% of lignin was not employed for the MB removal as the foam had lower

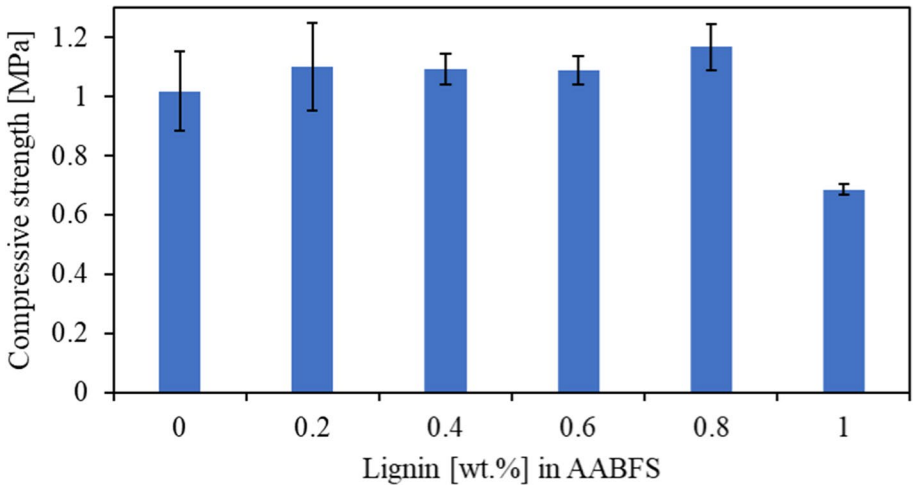

Fig. 5 Comparison of compressive strength of AABFS foam for the incorporation of different amount of lignin

mechanical strength. Figure 6 shows the effect of the amount of lignin in AABFS on MB removal performance. As the lignin amount was increased, the MB adsorption amount increased up to ~ 93% with the 0.8 wt% lignin addition in comparison to the AABFS without lignin. This is likely due to introduction of various functional groups to the surface, for example, ether, carbonyl, and aromatic hydroxyl groups, which can form electrostatic and π–π interactions as well as hydrogen bonds with MB (Bai et al. 2020; Liu et al. 2021). These increased interactions likely contributed to a higher adsorption amount. A similar observation was reported in the literature for a sodium alginate/lignin composite (Chen et al. 2022). The MB removal (as %) by AABFS foams with different amounts of lignin (0−0.8 wt%) is presented in Fig. S8 (SI): the MB removal remained at > 85% until 2 h for the AABFS foam without lignin, whereas for the AABFS foam with 0.8 wt% of lignin it was 100%.

The adsorption of MB was confirmed also with FTIR analysis of AABFS-Lig composite before and after MB adsorption (Fig. S9). A weak band at around ~ 2507 cm^{-1} was observed after MB adsorption by AABFS-Lig, which could be attributed as C_{het}–$N(CH_3)_2$ vibrations from the MB structure (Ovchinnikov et al. 2016). Two weak bands at ~ 1405 cm^{-1} and ~ 1480 cm^{-1} would be because of C–C stretching vibration and CH_2 scissoring in lignin respectively (Piqueras et al. 2020).

The AABFS-Lig composite foam with 0.8 wt% of lignin was selected to study the effect of influent MB concentration. With an increase in the concentration

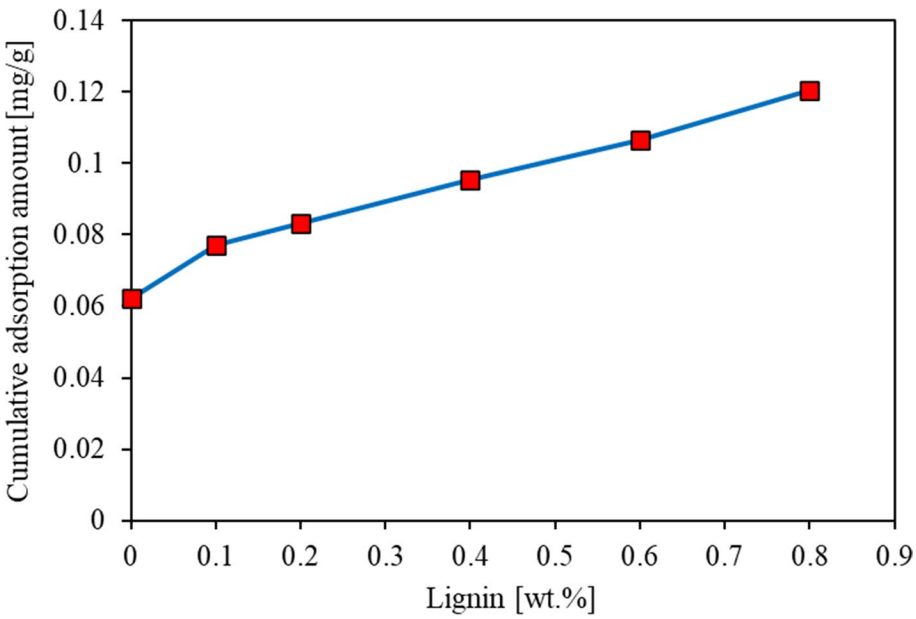

Fig. 6 The effect of lignin amount in AABFS foam on the MB cumulative adsorption amount. Cumulative adsorption amount was calculated in a 2 h experiment. Two litres of MB solution (5 mg/L, pH of 7) were passed through the foam with a 1 L/h flow rate

of MB, the cumulative adsorption amount (calculated at 6 h) of the foam increased almost linearly shown in Fig. 7. Again, it should be noted that since the mass of the foam includes approximately 2–3 wt% of water, the actual adsorption amount was higher than the reported values. The MB removal (as %) is shown in Fig. S10 (SI): after a 6 h experiment, the removal-% for the initial MB concentration of 100 mg/L decreased to 82%, while for the initial concentration of 10 mg/L it was 92%.

To observe the complete saturation and the subsequent maximum adsorption capacity of the optimized foam (i.e. AABFS with Triton X-114 and 0.8 wt% of lignin), an adsorption experiment of 73 h was conducted with a 100 mg/L MB solution using a flow rate of 1 L/h and pH of 7. The experimental data was fitted to the Adams–Bohart, Thomas, and Yoon–Nelson models and the obtained parameters are listed in Table 1. The Adams–Bohart model assumes the correlation between the bed depth and the breakthrough time. The Thomas model assumes that the data follows the Langmuir isotherm and kinetics model of the second order. The Yoon–Nelson model assumes that the adsorption is proportional to the reduction in the adsorption amount (Mekonnen et al. 2021). The R^2 values (both 0.97) for the Thomas and Yoon–Nelson models are higher than for the Adams–Bohart model ($R^2 = 0.85$), which indicates a better agreement between the experimental and calculated results for the Thomas and Yoon–Nelson models, and thus these are discussed below. The q_0 value for the Thomas model is 39.5 mg/g, which indicates the maximum adsorption capacity (in fact, the maximum adsorption capacity would be yet higher as the foam mass includes some weight of water) of the foam until complete saturation. This maximum adsorption capacity is higher than those reported for other alkali-activated foam materials, as shown in Table 2. From the Yoon–Nelson model, the parameter τ was estimated to be ~ 2262 min (corresponding to 37.7 L of treated water with 100 mg/L MB concentration and a foam mass of 96.7 g mass), which indicates the time needed for a 50% breakthrough. Figure 8 presents non-linear plots of the Adams–Bohart, Thomas, and Yoon–Nelson models fitted to the experimental data.

Table 1 Parameters of Adams–Bohart, Thomas, and Yoon–Nelson models for 100 mg/L MB influent, 1 L/h flow rate, and pH of 7

Model	Parameters	Calculated value
Adams–Bohart	k_{AB} [L/(mg × min)]	3.15×10^{-6}
	F (cm/min)	1.15
	N_0 (mg/L)	51559
	R^2	0.85
Thomas	K_{Th} [L/(min × mg)]	8.46×10^{-6}
	q_0 (mg/g)	39.5
	R^2	0.97
Yoon–Nelson	k_{YN} (L/min)	0.0009
	τ (min)	2262
	R^2	0.97

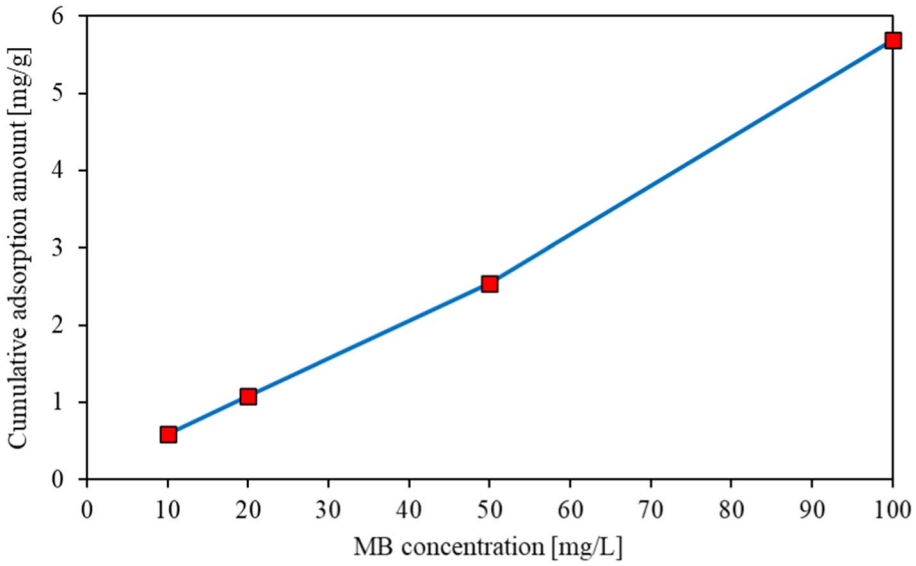

Fig. 7 The effect of initial MB concentration on the cumulative adsorption amount on AABFS with 0.8 wt% lignin, which was calculated after 6 h (flow rate of 1 L/h and pH of 7)

Table 2 A comparison of MB adsorption capacities for different alkali-activated foam materials in the literature to the current study

Precursor for alkali-activated foam adsorbent	Maximum adsorption capacity of MB (mg/g)	Pore-forming agent	References
Biomass fly ash	15.4	H_2O_2	Novais et al. 2018
Biomass fly ash	0.66	Al	Capela et al. 2022
Hypergolic coal gangue	9.4	Soyabean oil	Li et al. 2023
Metakaolin	7.8	H_2O_2	Kaya-Özkiper et al. 2022b
Metakaolin	4.9	–	Rożek et al. 2020
Fly ash	< 1	Al powder	Wattanasiriwech et al. 2021
Bauxite residue	17	Al powder	Hertel et al. 2019
Blast furnace slag	39.5	H_2O_2	Current study

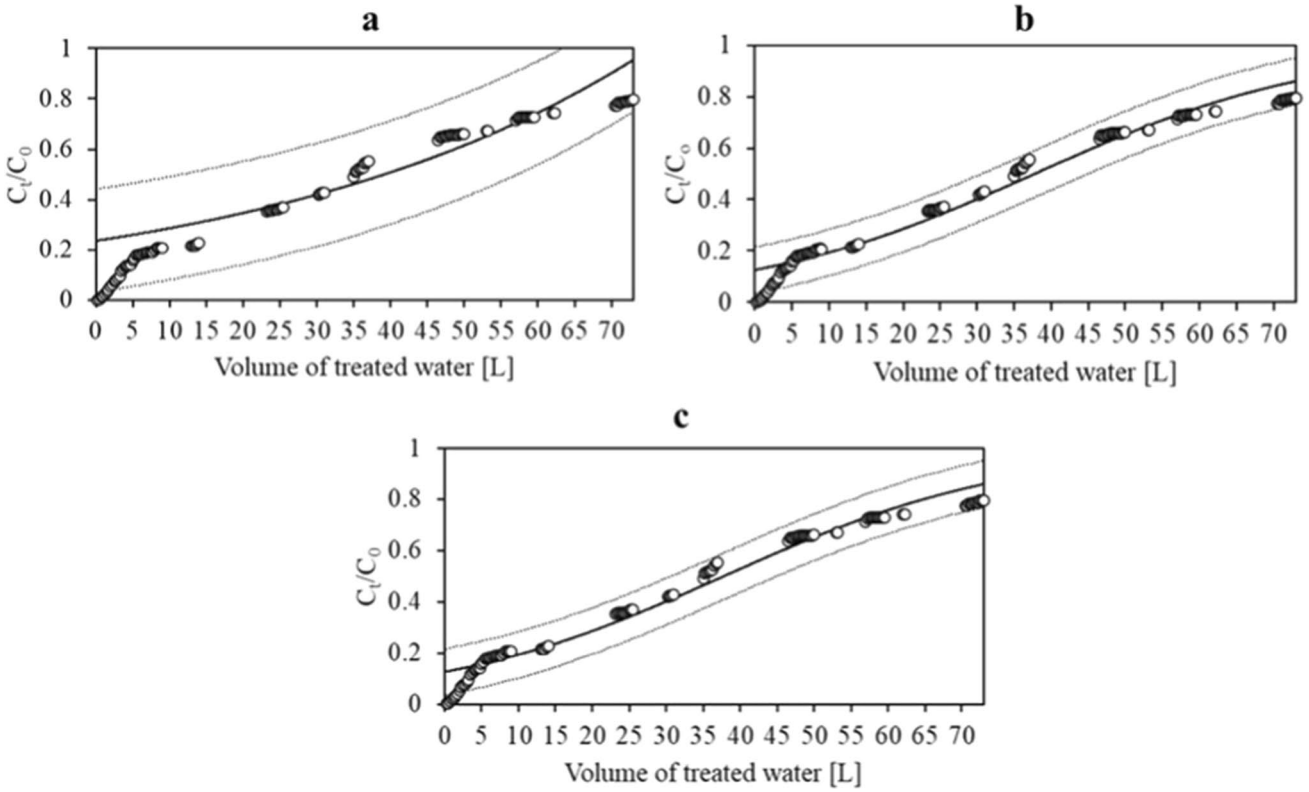

Fig. 8 Fitting of **a** the Adams–Bohart, **b** Thomas, and **c** Yoon–Nelson models to the experimental breakthrough curves (○ = C_t/C_0 experimental, — = C_t/C_0 calculated, •••••• = 95% upper and lower confidence limits)

Conclusion

In this study, the effect of different surfactants in the alkali-activation and direct foaming of blast furnace slag were assessed when the obtained foams were used in MB removal in dynamic adsorption experiments. The surfactant type (cationic, non-ionic, and the chain length of the surfactant) affects the porosity and pore structures in the obtained foams, but no evidence was found about the integration of the surfactant molecules to the structures of the foams after they were hardened and flushed with acetic acid. The highest adsorption performance was observed with a non-ionic surfactant, Triton X-114, which was selected for the optimization of operational parameters of dynamic adsorption (i.e., initial concentration of MB, flow rate, and pH).

Furthermore, lignin was introduced into the alkali-activated foam with an aim to enhance the adsorption performance. The optimum lignin addition amount was 0.8 wt% (in the range of 0–1 wt%). The incorporation of lignin in the foam significantly improved the adsorption performance as a ~93% increase in the adsorption amount of MB was

observed in comparison to the foam without lignin. The highest adsorption capacity for the lignin containing AABFS was 39.5 mg/g, which is among the highest reported for alkali-activated monolithic and/or foam structures.

Limitations of the present study include that not all parameters affecting adsorption were assessed for lignin-containing AABFS in details. Furthermore, regeneration of the composite foam containing AABFS and lignin after adsorption of MB was not investigated in this study. However, this study provides a preliminary proof-of-concept for the enhancement of MB adsorption by a composite foam containing AABFS and lignin.

Supplementary Information The online version contains supplementary material available at https://doi.org/10.1007/s13762-023-05245-5.

Acknowledgements This work was supported by the University of Oulu and the Academy of Finland Profi5 326291. The Center for Material Analysis at the University of Oulu is acknowledged for providing access to analytical instruments. Authors are grateful to Professor Mirja Illikainen for her contribution to funding acquisition.

Author contributions MAHB: Experimentation plan, experimental work, data analysis, data curation, writing (original draft). TL: Supervision, experimentation plan, resources, funding acquisition, project administration, writing (review and editing).

Funding Open Access funding provided by University of Oulu (including Oulu University Hospital).

Availability of data and materials Data will be available from the corresponding author on request.

Declarations

Conflict of interest The authors declare that they have no known competing financial interests or personal relationships that could have appeared to influence the work reported in this paper.

Ethical approval Not applicable.

Consent to participate All authors of this manuscript have consent to submit this manuscript to the "International Journal of Environmental Science and Technology".

Consent to publish All authors give consent to publish this manuscript upon acceptance.

References

Abdelbasir SM, Khalek MAA (2022) From waste to waste: iron blast furnace slag for heavy metal ions removal from aqueous system. Environ Sci Pollut Res 29:57964–57979. https://doi.org/10.1007/s11356-022-19834-3

Açışlı Ö, Acar İ, Khataee A (2022) Preparation of a surface modified fly ash-based geopolymer for removal of an anionic dye: parameters and adsorption mechanism. Chemosphere 295:133870. https://doi.org/10.1016/j.chemosphere.2022.133870

Ahmed FS, Alsaffar MA, AbdulRazak AA (2022) One-step synthesis of magnetic fly ash composites for methylene blue removal: batch and column study. Environ Sci Pollut Res. https://doi.org/10.1007/s11356-022-23491-x

Alves de Lima RO et al (2007) Mutagenic and carcinogenic potential of a textile azo dye processing plant effluent that impacts a drinking water source. Mutat Res Genet Toxicol Environ Mutagen 626:53–60. https://doi.org/10.1016/j.mrgentox.2006.08.002

Aziz IH et al (2020) Microstructure and porosity evolution of alkali activated slag at various heating temperatures. J Mater Res Technol 9:15894–15907. https://doi.org/10.1016/j.jmrt.2020.11.041

Bai C, Colombo P (2018) Processing, properties and applications of highly porous geopolymers: a review. Ceram Int 44:16103–16118. https://doi.org/10.1016/j.ceramint.2018.05.219

Bai H, Chen J, Zhou X, Hu C (2020) Single and binary adsorption of dyes from aqueous solutions using functionalized microcrystalline cellulose from cotton fiber. Korean J Chem Eng 37:1926–1932. https://doi.org/10.1007/s11814-020-0621-3

Bajwa DS et al (2019) A concise review of current lignin production, applications, products and their environmental impact. Ind Crops Prod 139:111526. https://doi.org/10.1016/j.indcrop.2019.111526

Banerjee S et al (2015) Rapid scavenging of methylene blue dye from a liquid phase by adsorption on alumina nanoparticles. RSC Adv 5:14425–14440. https://doi.org/10.1039/C4RA12235F

Bernal S et al (2015) Performance at high temperature of alkali-activated slag pastes produced with silica fume and rice husk ash based activators. Mater Constr 65:1–10

Bhuyan MAH et al (2022) Preparation of filter by alkali activation of blast furnace slag and its application for dye removal. J Environ Chem Eng 10:107051. https://doi.org/10.1016/j.jece.2021.107051

Bhuyan MAH et al (2023) Peracetic acid as a novel blowing agent in the direct foaming of alkali-activated materials. Appl Clay Sci 231:106727. https://doi.org/10.1016/j.clay.2022.106727

Bohart GS, Adams EQ (1920) Some aspects of the behavior of charcoal with respect to chlorine. J Am Chem Soc 42:523–544. https://doi.org/10.1021/ja01448a018

Cao R et al (2020) Interpreting the early-age reaction process of alkali-activated slag by using combined embedded ultrasonic measurement, thermal analysis, XRD FTIR and SEM. Compos B Eng 186:107840. https://doi.org/10.1016/j.compositesb.2020.107840

Capela MN et al (2022) Biomass fly ash self-hardened adsorbent monoliths for methylene blue removal from aqueous solutions. Appl Sci 12:5134. https://doi.org/10.3390/app12105134

Chan CH et al (2015) Cellulose nanofibrils: a rapid adsorbent for the removal of methylene blue. RSC Adv 5:18204–18212. https://doi.org/10.1039/C4RA15754K

Chavan RB (2011) 16-Environmentally friendly dyes. In: Clark M (ed) Handbook of textile and industrial dyeing. Woodhead Publishing, pp 515–561

Chen T et al (2022) efficient removal of methylene blue by bio-based sodium alginate/lignin composite hydrogel Beads. Polymers 14:2917. https://doi.org/10.3390/polym14142917

Cheng J et al (2020) Highly efficient removal of methylene blue dye from an aqueous solution using cellulose acetate nanofibrous

membranes modified by polydopamine. ACS Omega 5:5389–5400. https://doi.org/10.1021/acsomega.9b04425
Cruz-Olivares J et al (2013) Modeling of lead (II) biosorption by residue of allspice in a fixed-bed column. Chem Eng J 228:21–27. https://doi.org/10.1016/j.cej.2013.04.101
Ebadollahzadeh H, Zabihi M (2020) Competitive adsorption of methylene blue and Pb (II) ions on the nano-magnetic activated carbon and alumina. Mater Chem Phys 248:122893. https://doi.org/10.1016/j.matchemphys.2020.122893
Eftekhari M et al (2021) Statistical optimization, soft computing prediction, mechanistic and empirical evaluation for fundamental appraisal of copper, lead and malachite green adsorption. J Ind Inf Integr 23:100219. https://doi.org/10.1016/j.jii.2021.100219
El Alouani M, Saufi H, Moutaoukil G et al (2021) Application of geopolymers for treatment of water contaminated with organic and inorganic pollutants: state-of-the-art review. J Environ Chem Eng 9:105095. https://doi.org/10.1016/j.jece.2021.105095
Eldeeb TM et al (2022) Adsorption of methylene blue (MB) dye on ozone, purified and sonicated sawdust biochars. Biomass Conv Bioref. https://doi.org/10.1007/s13399-022-03015-w
Gautam RK et al (2014) Chapter 1. Contamination of heavy metals in aquatic media: transport, toxicity and technologies for remediation. In: Sharma S (ed) Heavy metals in water. R Soc Chem, Cambridge, pp 1–24
Gheibi M et al (2022) Mechanistic evaluation of cationic dyes adsorption onto low-cost calcinated aerated autoclaved concrete wastes. Int J Environ Sci Technol 19:6429–6444. https://doi.org/10.1007/s13762-021-03576-9
Ginimuge P, Jyothi S (2010) Methylene blue: revisited. J Anaesthesiol Clin Pharmacol 26:517. https://doi.org/10.4103/0970-9185.74599
Gunasekara C et al (2015) Zeta potential, gel formation and compressive strength of low calcium fly ash geopolymers. Constr Build Mater 95:592–599. https://doi.org/10.1016/j.conbuildmat.2015.07.175
Gupta VK, Suhas (2009) Application of low-cost adsorbents for dye removal—a review. J Environ Manage 90:2313–2342. https://doi.org/10.1016/j.jenvman.2008.11.017
Hertel T et al (2019) Use of modified bauxite residue-based porous inorganic polymer monoliths as adsorbents of methylene blue. J Clean Prod 227:877–889. https://doi.org/10.1016/j.jclepro.2019.04.084
Hou C, Hu B, Zhu J (2018) Photocatalytic degradation of methylene blue over TiO_2 pretreated with varying concentrations of NaOH. Catalysts 8:575. https://doi.org/10.3390/catal8120575
Humberto Tommasini Vieira Ramos FJ et al (2022) Performance of geopolymer foams of blast furnace slag covered with poly(lactic acid) for wastewater treatment. Ceram Int 48:732–743. https://doi.org/10.1016/j.ceramint.2021.09.153
Hunger K (2007) Industrial dyes: chemistry, properties Applications. Wiley, Germany
Hussain S et al (2020) Contamination of water resources by food dyes and its removal technologies. Water Chem. https://doi.org/10.5772/intechopen.90331
Joseph A et al (2019) Effective degradation of methylene blue in aqueous solution using Pd-supported Cu-doped Ti-pillared montmorillonite catalyst. Appl Clay Sci 168:7–10. https://doi.org/10.1016/j.clay.2018.10.009
Kadam AA et al (2011) Decolorization of adsorbed textile dyes by developed consortium of *Pseudomonas* sp. SUK1 and Aspergillus ochraceus NCIM-1146 under solid state fermentation. J Hazard Mater 189:486–494. https://doi.org/10.1016/j.jhazmat.2011.02.066
Kaya-Özkiper K, Uzun A, Soyer-Uzun S (2022a) A novel alkali activated magnesium silicate as an effective and mechanically strong adsorbent for methylene blue removal. J Hazard Mater 424:127256. https://doi.org/10.1016/j.jhazmat.2021.127256
Kaya-Özkiper K, Uzun A, Soyer-Uzun S (2022b) Tuning adsorption, structure and compressive strength of sepiolite- and metakaolin-based alkali activated monoliths for methylene blue removal from waste water. Surf Interfaces 33:102110. https://doi.org/10.1016/j.surfin.2022.102110
Khan I et al (2022) Review on methylene blue: its properties, uses toxicity and photodegradation. Water 14:242. https://doi.org/10.3390/w14020242
Kosswattaarachchi AM, Cook TR (2018) Repurposing the industrial dye methylene blue as an active component for redox flow batteries. ChemElectroChem 5:3437–3442. https://doi.org/10.1002/celc.201801097
Koyuncu H, Kul AR (2020) Removal of methylene blue dye from aqueous solution by nonliving lichen (*Pseudevernia furfuracea* (L.) Zopf.), as a novel biosorbent. Appl Water Sci 10:72. https://doi.org/10.1007/s13201-020-1156-9
Kuang Y, Zhang X, Zhou S (2020) Adsorption of methylene blue in water onto activated carbon by surfactant modification. Water 12:587. https://doi.org/10.3390/w12020587
Latorrata S, Balzarotti R, Adami MI et al (2021) Wastewater treatment using alkali-activated-based sorbents produced from blast furnace slag. Appl Sci 11:2985. https://doi.org/10.3390/app11072985
Li X et al (2023) Porous alkali-activated material from hypergolic coal gangue by microwave foaming for methylene blue removal. J Am Ceram 106:1473–1489. https://doi.org/10.1111/jace.18812
Liu X-J, Li M-F, Singh SK (2021) Manganese-modified lignin biochar as adsorbent for removal of methylene blue. J Mater Res Technol 12:1434–1445. https://doi.org/10.1016/j.jmrt.2021.03.076
Luukkonen T et al (2022) Water disinfection with geopolymer–bentonite composite foam containing silver nanoparticles. Mater Lett 311:131636. https://doi.org/10.1016/j.matlet.2021.131636
Luukkonen T et al (2016) Simultaneous removal of Ni(II), As(III), and Sb(III) from spiked mine effluent with metakaolin and blast-furnace-slag geopolymers. J Environ Manag 166:579–588. https://doi.org/10.1016/j.jenvman.2015.11.007
Maleki A et al (2020) Adsorbent materials based on a geopolymer paste for dye removal from aqueous solutions. Arab J Chem 13:3017–3025. https://doi.org/10.1016/j.arabjc.2018.08.011
Mariana M et al (2021) A current advancement on the role of lignin as sustainable reinforcement material in biopolymeric blends. J Mater Res Technol 15:2287–2316. https://doi.org/10.1016/j.jmrt.2021.08.139
Medina TJ et al (2020) Microstructure and Pb^{2+} adsorption properties of blast furnace slag and fly ash based geopolymers. Minerals 10:808. https://doi.org/10.3390/min10090808
Mekonnen DT, Alemayehu E, Lennartz B (2021) Fixed-bed column technique for the removal of phosphate from water using leftover coal. Materials 14:5466. https://doi.org/10.3390/ma14195466
Moradihamedani P (2022) Recent advances in dye removal from wastewater by membrane technology: a review. Polym Bull 79:2603–2631. https://doi.org/10.1007/s00289-021-03603-2
Nasuha N, Hameed BH, Din ATM (2010) Rejected tea as a potential low-cost adsorbent for the removal of methylene blue. J Hazard Mater 175:126–132. https://doi.org/10.1016/j.jhazmat.2009.09.138
Novais RM et al (2018) Biomass fly ash geopolymer monoliths for effective methylene blue removal from wastewaters. J Clean Prod 171:783–794. https://doi.org/10.1016/j.jclepro.2017.10.078
Oladoye PO et al (2022) Methylene blue dye: toxicity and potential elimination technology from wastewater. Results Eng 16:100678. https://doi.org/10.1016/j.rineng.2022.100678
Ortúzar M et al (2022) Pharmaceutical pollution in aquatic environments: a concise review of environmental impacts and

bioremediation systems. Front Microbiol. https://doi.org/10.3389/fmicb.2022.869332
Ovchinnikov OV et al (2016) Manifestation of intermolecular interactions in FTIR spectra of methylene blue molecules. Vib Spectrosc 86:181–189. https://doi.org/10.1016/j.vibspec.2016.06.016
Pandey A, Singh P, Iyengar L (2007) Bacterial decolorization and degradation of azo dyes. Int Biodeterior Biodegrad 59:73–84. https://doi.org/10.1016/j.ibiod.2006.08.006
Pang J et al (2017) Adsorption behaviors of methylene blue from aqueous solution on mesoporous birnessite. J Taiwan Inst Chem Eng 77:168–176. https://doi.org/10.1016/j.jtice.2017.04.041
Parakala S, Moulik S, Sridhar S (2019) Effective separation of methylene blue dye from aqueous solutions by integration of micellar enhanced ultrafiltration with vacuum membrane distillation. Chem Eng J 375:122015. https://doi.org/10.1016/j.cej.2019.122015
Patisson F, Mirgaux O (2020) Hydrogen ironmaking: how it works. Metals 10:922. https://doi.org/10.3390/met10070922
Perumal P et al (2021) Role of surfactants on the synthesis of impure kaolin-based alkali-activated, low-temperature porous ceramics. Open Ceram 6:100097. https://doi.org/10.1016/j.oceram.2021.100097
Piqueras S et al (2020) Understanding the formation of heartwood in larch using synchrotron infrared imaging combined with multivariate analysis and atomic force microscope infrared spectroscopy. Front Plant Sci. https://doi.org/10.3389/fpls.2019.01701
Puertas F et al (2011) A model for the C–A–S–H gel formed in alkali-activated slag cements. J Eur Ceram 31:2043–2056. https://doi.org/10.1016/j.jeurceramsoc.2011.04.036
Quesada HB et al (2019) Surface water pollution by pharmaceuticals and an alternative of removal by low-cost adsorbents: a review. Chemosphere 222:766–780. https://doi.org/10.1016/j.chemosphere.2019.02.009
Raza W et al (2019) Removal of phenolic compounds from industrial waste water based on membrane-based technologies. J Ind Eng Chem 71:1–18. https://doi.org/10.1016/j.jiec.2018.11.024
Razeghi HR, Ghadir P, Javadi AA (2022) Mechanical strength of saline sandy soils stabilized with alkali-activated cements. Sustainability 14:13669. https://doi.org/10.3390/su142013669
Rezaei M, Salem S (2016) Photocatalytic activity enhancement of anatase–graphene nanocomposite for methylene removal: degradation and kinetics. Spectrochim Acta A Mol Biomol Spectrosc 167:41–49. https://doi.org/10.1016/j.saa.2016.04.057
Rożek P, Król M, Mozgawa W (2020) Lightweight geopolymer-expanded glass composites for removal of methylene blue from aqueous solutions. Ceram Int 46:19785–19791. https://doi.org/10.1016/j.ceramint.2020.05.011
Runtti H et al (2016) Sulphate removal over barium-modified blast-furnace-slag geopolymer. J Hazard Mater 317:373–384. https://doi.org/10.1016/j.jhazmat.2016.06.001
Saad R, Hawari J (2013) Grafting of lignin onto nanostructured silica SBA-15: preparation and characterization. J Porous Mater 20:227–233. https://doi.org/10.1007/s10934-012-9592-z
Salazar-Rabago JJ et al (2017) Biosorption mechanism of methylene blue from aqueous solution onto White Pine (*Pinus durangensis*) sawdust: effect of operating conditions. Sustain Environ Res 27:32–40. https://doi.org/10.1016/j.serj.2016.11.009
Sharma A et al (2021) Economical concerns of lignin in the energy sector. Clean Eng Technol 4:100258. https://doi.org/10.1016/j.clet.2021.100258
Shorey R, Gupta A, Mekonnen TH (2021) Hydrophobic modification of lignin for rubber composites. Ind Crops Prod 174:114189. https://doi.org/10.1016/j.indcrop.2021.114189
Sittipol W, Sronsri C, U-yen K (2021) Effect of magnetic fields on the efficiency of the photocatalytic degradation of methylene blue in a dynamic fluid system. J Clean Prod 325:129284. https://doi.org/10.1016/j.jclepro.2021.129284
Subramanian H, Krishnan M, Mahalingam A (2022) Photocatalytic dye degradation and photoexcited anti-microbial activities of green zinc oxide nanoparticles synthesized via Sargassum muticum extracts. RSC Adv 12:985–997. https://doi.org/10.1039/D1RA08196A
Sundhararasu E et al (2021) Alkali-activated adsorbents from slags: column adsorption and regeneration study for nickel(II) removal. ChemEngineering 5:13. https://doi.org/10.3390/chemengineering5010013
Suteu D, Malutan T, Bilba D (2010) Removal of reactive dye brilliant red HE-3B from aqueous solutions by industrial lignin: equilibrium and kinetics modeling. Desalination 255:84–90. https://doi.org/10.1016/j.desal.2010.01.010
Thomas HC (1944) Heterogeneous ion exchange in a flowing system. J Am Chem Soc 66:1664–1666. https://doi.org/10.1021/ja01238a017
Wainwright M et al (1997) Increased cytotoxicity and phototoxicity in the methylene blue series via chromophore methylation. J Photochem Photobiol b: Biol 40:233–239. https://doi.org/10.1016/S1011-1344(97)00061-4
Walker DB et al (2019) Chapter 16-Surface water pollution. In: Brusseau ML, Pepper IL, Gerba CP (eds) Environmental and pollution science (third edition). Academic Press, pp 261–292
Wang S, Chen X, Yin Y et al (2022) Lignin-based hydrogels for efficient dye removal via synergistic effect of multiple interactions. Ind Crops Prod 189:115840. https://doi.org/10.1016/j.indcrop.2022.115840
Wattanasiriwech D, Yomthong K, Wattanasiriwech S (2021) Adsorption efficiency and photocatalytic activity of fly ash-based geopolymer foam mortar. Ceram Int 47:27361–27371. https://doi.org/10.1016/j.ceramint.2021.06.158
Yao Z, Wang L, Qi J (2009) Biosorption of methylene blue from aqueous solution using a bioenergy forest waste: *Xanthoceras sorbifolia* seed coat. CLEAN—Soil Air Water 37:642–648. https://doi.org/10.1002/clen.200900093
Ye H, Zhang Y, Yu Z, Mu J (2018) Effects of cellulose, hemicellulose, and lignin on the morphology and mechanical properties of metakaolin-based geopolymer. Constr Build Mater 173:10–16. https://doi.org/10.1016/j.conbuildmat.2018.04.028
Ye HY et al (2023) Highly efficient removal of organic dyes and heavy metal cation from wastewater by polyphenolate porous coordination polymer. Int J Environ Sci Technol. https://doi.org/10.1007/s13762-023-04858-0
Yoon YH, Nelson JH (1984) Application of gas adsorption kinetics—II. A theoretical model for respirator cartridge service life and its practical applications. Am Ind Hyg Assoc J 45:517–524. https://doi.org/10.1080/15298668491400205
Zamora-Ledezma et al (2021) Heavy metal water pollution: a fresh look about hazards, novel and conventional remediation methods. Environ Technol Innov 22:101504. https://doi.org/10.1016/j.eti.2021.101504